Relationship between outbursts and nuclear splitting of comet 73P/Schwassmann-Wachmann 3*

Z. Sekanina[1], H. Boehnhardt[2], H. U. Käufl[3], and K. Birkle[4]

[1] Jet propulsion Laboratory, California Institute of Technology, 183.501, 4800 oak Grove Drive, Pasadena, CA 91109, U.S.A.
[2] Universit äts-Sternwarte, Schreinerstr. 1, D-81679 München Federal Republic of Germany
[3] European Southern Observatory, Karl-Schwarzschild-Str 2, D85748 Garching bei München, Federal Republic of Germany
[4] Max-Planck-Insti tut für Astronomie, Königstuhl 17, D 691 r Heidelberg, Federal Republic of Germany

Abstract. The major outburst of 73P/Schwassmann Wachmann 3, detected ~2 weeks before perihelion as a sudden increase in the production of hydroxyl, is found to have been followed by a steady brightening in the visible light until ~20 days past perihelion, when the comet was a factor of ~200 more luminous than in its quiescent phase. When 80 days after perihelion the nucleus, whose effective diameter is estimated at ~3 km, appeared to be triple (with unconfirmed reports of up to four additional companions), the issue of primary interest was the nature of the relationship between the splitting and the initial stages of the outburst. Application of a standard model for the split cornets indicates that, nominally, the first breakup the separation of the component B from the principal nucleus C (the easternmost component) - occurred most probably in late October, some six weeks following the outburst's onset. A secondary breakup - the separation of A (the westernmost component) from C - followed some two weeks later. These fragmentation episodes correlate well with two less prominent, secondary flare-ups on the light curve. Also examined are the circumstances of separation for the four additional, suspected companions. The inferred delayed response of the nucleus to the major disturbance on its surface is a phenomenon not previously reported for any other split comet. It was proposed in the' early 1980s that some companion nuclei of nonfidally split comets may represent large, nearly inert fragments of the surface mantle of refractory material that were torn off, thus exposing the previously protected reservoir of ice beneath. If so, the case of P/Schwassmann-Wachmann 3 suggests that the disturbed area of the mantle first released considerable amounts of dust, microscopic grains in particular - hence, an outburst. The separation of a large fragment (or fragments) of the mantle apparently required continuing, more sustained manifestations of elevated activity (triggered possibly by a buildup of vapor pressure in localized subsurface pockets of confined volatilized ices), in order to overcome the resistence to fracture offered by intrinsic cohesion of the nucleus and its mantle. In any case, the delayed response provides strong evidence against models of a strengthless cometary nucleus.

Key words: comet 73P/Schwassmann-Wachmann 3 – nuclear splitting differential nongravitational effects - outbursts light curve

Send offprint requests to: Zdenek Sekanina

* Based on observations made at the European Southern Observatory, Chile, and at the Calar Alto Observatory, Spain

1. Introduction

Comet Schwassmann Wachmann 3, which had until recently been known as one of the intrinsically faint periodic comets of the Jupiter family, has a relatively short history, even though it was discovered as long ago as 1930. Unfortunately, the object was lost following this discovery apparition and remained unobserved until 1979, with eight missed returns to the Sun during the intervening period of 49 years (Belyaev & Shaporev 1975, Landgraf 1983). Again avoiding detection in the course of the unfavorable return of 1984/5, the comet was recovered during its next approach to the Sun in 1990, when it was observed extensively. Thus, the 1995/6 apparition only was the object's fourth recorded return to the Sun.

Yet, two of the four apparitions are memorable because of the comet's unusual appearance. on May 31, 1930, $13\frac{1}{2}$ days before perihelion, P/Schwassmann-Wachmann 3 missed Earth by only 9.2 million km and for several days was a fairly bright object on the verge of detection with naked eye. During May-July 1930, the comet displayed a sunward fan (described by some observers as an elongated nuclear condensation at larger geocentric distances) and in May, in addition, a straight tail that pointed in the direction away from the Sun. Schüller's (1930) visual detection of a double nucleus in late May 1930 was never

confirmed by other observers, including those using large telescopes of the time.

The comet's physical appearance in 1930, especially the reported temporal variations in the orientation of Its sunward fan-shaped extension were examined by Sekanina (1989a). The primary objective of that study was an interpretation of the fan in terms of a collimated flow of dust ejecta from one or more isolated sources It was concluded that the source(s) were situated within 20° of the sunlit pole of the comet's rotating nucleus and that temporal variations in the fan's orientation could successfully be modelled only on the premise of a rapid motion of the spin axis. Between mid-April and late July 1930, the average and peak precession rates were found to be equal to, respectively, 0°.9 and 1°.4 per day. The active surface area was crudely estimated at 0.8 km^2 and the nucleus was presumed to be strongly nonspherical.

The apparition of 1979 was not very favorable, as the comet remained more than 1 AU from Earth at all times. The geometry was much better in 1990, when the comet approached Earth to 0.367 AU on April 17. The apparition of 1995/6 has actually been even less favorable than that of 1979, with the comet's geocentric distance always greater than 1.3 AU. However, because of the unexpected events, the comet became as bright as, or brighter than, at the time of closest approach in 1930. To investigate these events in detail, we examine the comet's light curve first

2. The comet's light curve in 1930 1996 and the major outburst of 1995

By the light curve of a comet one usually means a plot of total magnitudes reported by visual observers, normalized to 1 AU from Earth and converted, to the extent possible, to a uniform system by correcting for personal and instrumental effects. These observer/telescope corrections are essentially calibrated on the data reported by highly experienced observers and are believed to refer, within the observational uncertainties usually amounting to a few tenths of a magnitude, to a total visual brightness that is intrinsic to the object. The composite light curve of 73P/Schwassmann-Wachmann 3, which is shown in Fig. 1, also includes three photographic and three charge-coupled-device (CCD) magnitudes, as described in the subsequent paragraphs. Before plotting them, we converted these data to the system of visual magnitudes, using approximate corrections based on the assumption that the color was dominated by particulates. The range of optical reflectivity gradients of cometary dust (e.g., Jewitt & Meech 1986) implies for the color index ($B-V$) of the standard UBV system (Johnson 1955) the values between +0.73 and +0.87 mag, equivalent to an average difference between the visual and the photographic magnitude, $m_{vis} - m_{pg} = -0.73 \pm 007$ mag (eg Kron & Mayall 1960). On the other hand, three different laws (Howarth & Bailey 1980, Feijth 1980, Stanton 1981) yield for the difference between m_{vis} and the V magnitude of the UBV system, $m_{vis} V = +0.1010 + 0.13$ msg.

The light curve in 1930 was examined by Sekanina (1989a). He noticed the presence of large discrepancies among magnitude estimates made by the various observers, which was caused by a prominent "delta effect". This effect, often involved in total visual magnitude estimates of comets at very small geocentric distances, is believed to be due to the human eye's inability to detect faint, outer fringes of a very extended object with an exceptionally low surface-intensity gradient. As a result, the observer underestimates the integrated brightness the more the larger (and therefore the closer) the object. However, the magnitude (If' the delta effect is both observer and instrument dependent, thus the large scatter among the observers. To avoid the pitfalls that attempts to account for this effect are likely to lead to, we do not include the light curve from this apparition in Fig. 1. For the sake of comparison with the other apparitions, however, we plot the intrinsically brightest, color-corrected magnitude estimate made photographically by Wood (1930) about 47 clays after perihelion, when the comet was already more than 0.4 AU from Earth and no significant delta effect should be involved.

Only four visual magnitude estimates are available from the apparition of 1979. Reported by Green (1980, 1981), they were made by two experienced observers, for whom the magnitude corrections are well known. One of them observed the comet with the same instrument again in 1990 These data are complemented in Fig. 1 with two photographic brightness estimates reported by Herald (1979), which were corrected for the color effect as discussed above.

A total of 106 magnitude estimates by 14 observers are plotted in Fig. 1 from the favorable apparition of 1990, covering the period from 60 days before perihelion to 45 days past perihelion (Green 1990, 1991, 1992, 1993, 1995a) At this apparition, the comet's light, curve was fairly smooth, peaking shortly after perihelion. The normalized brightness never exceeded magnitude 10. Comparison with the few data points from 1979 shows the comet to have been about equally bright intrinsically at the two apparitions The light curve in 1990 also appears to compare favorably with the brightest data point from 1930. Chen & Jewitt (1994) searched but did not detect any nuclear companions on May 14, 1990, 5 days before perihelion passage.

Following the comet's recovery at Calar Alto in late 1994 (Birkle et al. 1994), the object was observed at the European Southern Observatory (ESO) in March and June 1995, using the Danish 1.5 meter and the ESO/MPG 2.2-meter telescopes equipped with CCD detectors and the broad-band R filters of the Cousins photometric system. These observations were made as part of a program that has been monitoring temporal variations in the comet's physical appearance. They are summarized in Sect. 9, in

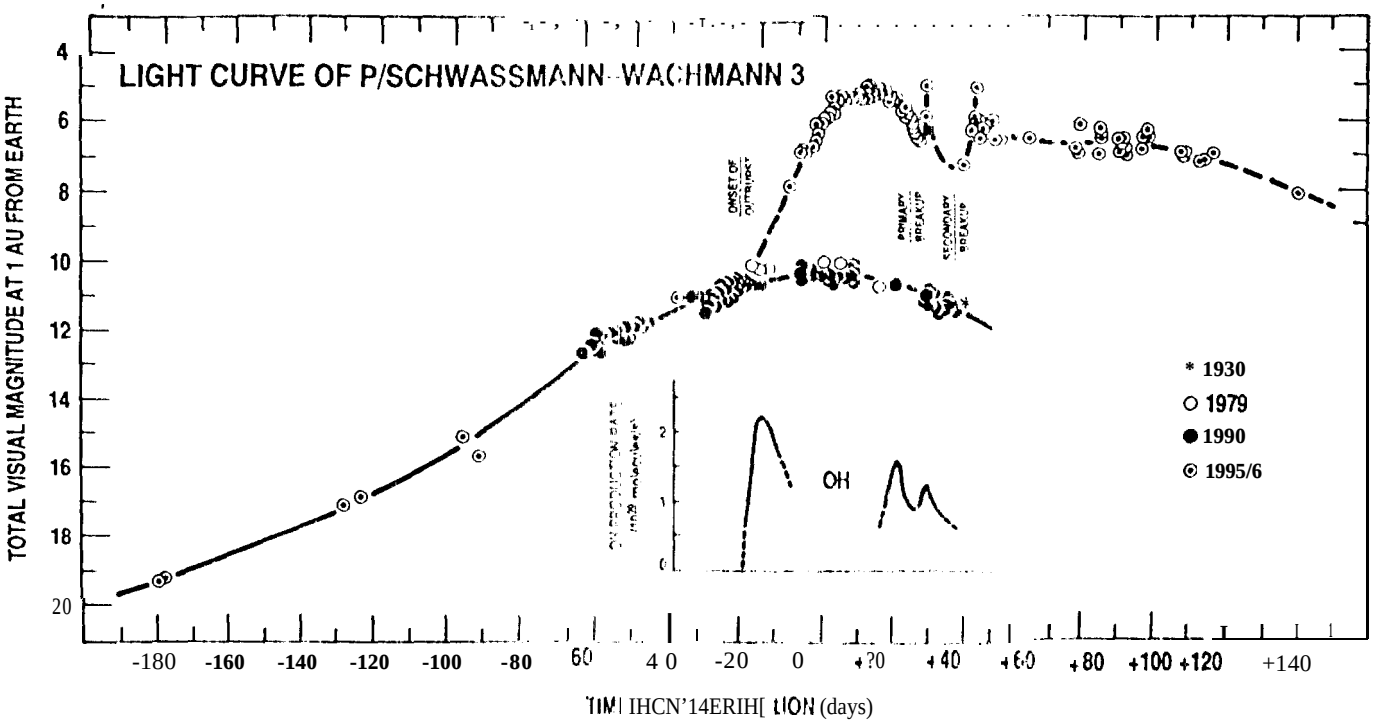

Fig. 1. **Visual light curve of P/Schwassmann-Wachmann 3. Indications are that at the earlier apparitions and until the time of major outburst in 1995, the comet's intrinsic brightness can be approximated by the same, smoothly varying law (solid curve). Since the outburst, the brightness has fluctuated erratically, exceeding the quiescent level by a factor of up to ~200 and** more (broken curve). The times of the outburst and of the separations of the components B and A **(Sect. 6) are depicted.** The OH **production curve by Crovisier et al,** (1996) is also plotted for comparison. The onset of **the outburst about 16 days before perihelion is consistently indicated by both the light curve and the OH production curve, but their temporal variations are dramatically different.**

connection with our study of the nuclear dimensions. We found a solar color for the practically bare nucleus at the time of recovery, $(V-R)_{Johnson} = +0.53 \pm 0.14$ mag, which is equivalent to $(V-R)_{Cousins} = +0.36 \pm 0.1$ (1 mag (Fernie 1983) and to $m_{vis} - R_{Cousins} = +(1.48:; 0.11$ mag. In Fig. 1 this correction was applied to the magnit 11111. from the La Sills images taken in March and June on which the comet is seen to have already been active and which were instrumental in establishing the general character of the light curve between ~180 and . ..90 days before perihelion. The visual observations began in mid May 1995, more than 120 days before perihelion, and continued through early February 1996, about 140 days after perihelion, as the comet was slowly approaching the conjunction with the Sun. A total of 100 magnitude determinations by 15 observers are included in Fig. 1. The great majority of them is from the tabulations by Green (1995b, 1996) with a few additional entries from Circulars of the International Astronomical Union.

Comparison of the 1995/96 light curve with those from the earlier apparitions shows the enormity of the outburst that commenced in early September 1995. This event was first reported by Crovisier et al. (1995) as a sudden, dramatic enhancement of a signal from the OH radio lines. From their observations they derived a peak hydroxyl production rate of $(2.22 \pm 0.22) \times 10^{29}$ mol/s on Sept. 11-13, compared with $(0.92 \pm 0.15) \times 10^{29}$ mol/s on Sept. 8 – 10 and with a 3σ upper limit of 0.28×10^{29} mol/s on Sept. 1-5 (Crovisier et al. 1996). Thus, the outburst - probably the first one ever detected by radio techniques before being seen visually - began in the period of Sept. 6-8, or 17 to 15 days before perihelion. This critical period of time is also indicated in Fig. 1 by back extrapolation of the subsequent visual observations of elevated brightness. The peak normalized magnitude of . . 5o was reached about 20 days past perihelion, some five weeks after the beginning of the outburst and during this period of time the intrinsic visual brightness grew by a factor of approximately 200. Additional short-lived flare-ups are apparent on both the OH production curve and the light curve during the following weeks, after which the brightness began to subside at a rate that is clearly much slower than that suggested by the undisturbed light curve during the 1990 apparition.

The two secondary peaks on the light curve are likely to be genuine flare-ups. However, since they are documented by very few data points, their amplitudes are necessarily uncertain and may be exaggerated in Fig. 1. The first of the two events, peaking about 35 days af-

ter perihelion, is based primarily on an experienced observer's account of the comet being at this time (and with the same instrument) 0.3 mag intrinsically brighter than 9 days earlier when its brightness was observed to be subsiding. Some flaring is further supported by the account of one of the most experienced observers, who, also 35 days after perihelion, found the comet 0.2 mag brighter than three days earlier. The strongest evidence for the second sharp brightening, about 49 days after perihelion, is a report by a fairly experienced observer that the comet faded by 1.4 mag during the next 24 hours, while another highly experienced observer found the comet to be much fainter 46 days after perihelion, between the two secondary peaks in Fig. 1. Regardless of the degree of significance of these two events, the comet's propensity for flaring up was obviously not limited to the single episode in early September 1995. Rather, it was followed try additional discrete eruptive events superimposed on an essentially continuous background of elevated activity. In the next section we describe what we consider the most dramatic product of the object's apparently continuing disintegration

3. Discovery and high-resolution observations of the multiple nucleus at ESO

The multiplicity of the nucleus of comet P/Schwassmann Wachmann 3 was first detected at ESO La Silla during an observing run of Dec. 12–14, 1995 (Boehnhardt & Kaufl 1995). The observations were made simultaneously with the 3.5-meter New Technology Telescope (NTT) using the EMMI instrument (visual focal reducer) in the optical wavelength range and with the 3.6-meter telescope using TIMMI (mid-infrared focal reducer) in the thermal infrared. Because of a very narrow observing window (Table 1), we focussed primarily on broadband imaging in the Kron-Cousins R passband at the NTT. A few exposures through the UBV and a CN emission band filters were also taken, as were low-dispersion spectra, but these results are not reported in this paper. A continuum 10 μm imaging (with a TIMMI N2 filter) was performed at the 3.6-meter telescope. For the flux calibration, we measured the photometric standard stars (Landolt 1992) and took separate, nearly simultaneous images of the sky about 1° to the north of the comet's center through the NTT broadband filters on Dec. 12 and 14. The images of Dec 13 could not be calibrated because of cirrus clouds. The N2 filter imaging of the comet was successful only on Dec. 12. During the following two nights, unstable atmospheric conditions together with problems in the telescope tracking prevented us from obtaining further useful data on P/Schwassmann-Wachmann 3 in the thermal infrared.

The major discovery of the NTT observations the detection of three separate brightness condensations in the coma is shown in Fig. 2(d). The individual components were aligned in a nearly rectilinear chain about 4 arcsec long and oriented approximately along the projected direction of the Sun-comet vector, whose position angle on Dec. 12, 1995 was 91°. To comply with the notation used on the *Minor Planet Circulars* (Sect. 4), we refer to the westernmost fragment as A, to the easternmost one as C, while the middle condensation is called B. A fourth brightness peak, located about 2 arcsec to the south of the component C is seen on the N2 images and, for reasons obvious from Sect 4, we refer to it as F [Fig. 2(c)]. Whereas the condensations A and C were detected in both the optical and the infrared wavelengths, the component B was seen only on the NTT exposures and F only in the infrared frames. On the broadband images, the discrete condensations were embedded in an extended coma, whose central part was strongly elongated along the radius vector. On the NTT images, isophotes of the outer coma's western end were wide and pointing in the direction of the Sun; a general interpretation of this phenomenon is offered in Sect. 8. The flux distribution in these images is evidently representative of the spatial density of dust particles in the coma, which differs dramatically from the almost circular isophotes in the CN images of a nearly isotropic gaseous expansion. The positional changes and brightness variations of the condensations A, B, and C with time are apparent from Fig. 2(d) through (g).

By courtesy of our colleagues observing at other ESO telescopes, additional UBVR images of the comet from late 1995 have become available to the authors, These CCD frames were taken by J Manfroid (Liège, Belgium) with the Dutch 0.9-meter and Danish 1.5-meter telescopes between Oct. 27 and Nov 1, by K. Reinsch (Göttingen, Germany) with the ESO/MPG 2.2-meter telescope on Nov. 28, and by J. Storm (ESO, Chile) with the Danish 1.5-meter telescope on Dec 1–2 (for details about the observing geometry and instrumentation, cf. Table 1). On these dates the general appearance of the cornet's inner coma resembled that seen on the NTT images in mid-December However, on the original frames the central brightness peaks, while appearing elongated approximately along the radius vector, could not be resolved into individual components.

After discovery of the nuclear fragments, further NTT images of the comet were obtained through a broadband R filter on Jan. 7 and 31, 1996 (Table 1). The lengths of the trail of the three fragments A, B, and C on the two dates were about 10 and 17 arcsec, respectively. By then, each fragment had its own coma and tail embedded in a common sheath of material [Fig. 2(f) and (g)]. The sunward coma continued to display a well pronounced sunward extension, as discussed in Sect. 8.

A detailed description of the collection of ESO images of the comet's nuclear fragments is offered by Boehnhardt et al. (1996). In all exposures, the telescope tracking was set to follow the object's calculated geocentric motion in the sky. For the images obtained between Oct. 27 and 11 (cf. 2, separate quasi-simultaneous sky background exposures are not available During photometric nights, how-

ever, standard stats were observed, so that the frame can be flux calibrated.

Data reduction and image deconvolution. The basic data reduction of the CCD images in the optical wavelength range involved bias level subtraction and flat-field division. The dark current contribution to the pixel counts was negligibly small. Where available the sky level correction was made by subtracting the corresponding mean count values obtained from the separate quasi-simultaneous sky exposures. In all other cases the sky background was approximated from the four star-free areas at the edge of the respective cornet exposures. When possible, standard stars were used for the photometrical calibration of the images, with the extinction correction (but not a color correction) applied.

The Richardson-Lucy algorithm (Richardson 1971; Lucy 1974) of the ESO MIDAS data reduction software package was applied to the images taken between late October and early December 1995 in order to resolve possible discrete condensations in the elongated central part of the coma. An artificial two-dimensional Gaussian point-spread function (PSF) was constructed by using the full width at-half-maximum (FWHM) derived from brightness cross profiles of star trails. Using the artificial PSF typically about 400 iterations were needed to obtain a stable result from the MIDAS sharpening procedure. In this fashion, the elongated central condensation could be resolved into two components on the best images taken between Nov. 28 and Dec. 2, 1995 [Boehnhardt et al. 1996 and Fig. 2(c), 1]. A similar deconvolution processing of the exposures from Oct. 27 to Nov. 1, 1995 failed to reveal separate condensations in the central peak, as seen on the best image from this series shown in Fig. 2(a). For an explanation of this negative result the reader is referred to Sect. 8.

Positional measurements. Whenever separate condensations were resolved in the coma, we measured the relative pixel offsets of the components with reference to the brightest condensation. For the NTT images (from Dec. 12 on) the identity of the condensations could easily be established from their configuration and brightness. The nucleus C at the eastern end of the chain always was the brightest component, the nucleus A at the western end the second brightest during December 1995, but fainter than the component B in the middle of the chain during January 1996 (Sect. 7). For the earlier images the identification of the components is a more difficult task which could only be settled by dynamically modelling the nuclear splitting (Sect. 6).

In practice, the positional measurements of the condensations were carried out by computing the central pixel coordinates of the circular area (approximately centered on the object in question) using an intensity weighted first moment of the flux values of the pixels in the aperture. Depending on the distance between the components the radius of the centering aperture was chosen between 3 and 6 pixels to avoid perturbations from brightness halo of the proximate condensation (or condensations). The positional measurements were repeated four times per object and image, each time with a new initial centering of the aperture. This procedure was repeated for consecutive exposures (if available) on each night. All such data were averaged to calculate the mean pixel coordinates of the components for the mid-exposure times.

Table 1 lists the separation distances among the condensations measured in the images available to the authors. The intrinsic error of these measurements, defined by the maximum deviation of the individual pixel coordinates of a single night data set from their mean values, was found to be 0.07 arcsec for the NTT images in December 1995, 0.05 arcsec for the January 1996 ones, and 0.2 arcsec for the early, non-NTT observations. It should be noted that the actual positional error could be larger than the intrinsic one because of pixel scale changes introduced by refocussing the telescope and/or the instrument during the nights involved. These changes have not been accounted for. The *maximum* scale factor changes in the NTT images are on the order of 1 percent. Therefore, depending on the pixel separation of the condensations, a systematic error in the positions of A relative to C of up to 0.04 arcsec in mid-December 1995 and up to 0.15 arcsec in late January 1996 could result from refocussing the optical system. Since this scale-factor error is propagating along the separation vector, it applies essentially to the offsets in right ascension. The corresponding uncertainties are substantially smaller in declination and also for the offsets of B relative to C. Because of the proximity of the condensations, the scale effects are negligible for the early images taken with the telescopes other than the NTT. The preliminary value for the separation distance, 1.4 arcsec between the two components on the Nov. 28 image, reported on IAU Circ. 6301, was due to inadvertent use of an incorrect pixel size of 0,52 arcsec; this error has now been corrected (Table 1). The photometric analysis is described in Sect. 8.

4 Additional information on the multiple nucleus

From Dec. 23, 1995 on, the multiple nucleus was observed (and the projected separation distances and orientations among the individual components measured) at several observatories worldwide, in particular, in Australia, Japan, Slovakia, and the United States (Arizona, Hawaii, and Texas), in addition to ESO La Sills. The offsets of the companions on most of these images were derived from the absolute positions collected and published by Marsden (1996). These tabulations also include magnitudes for some of the condensations reported by A. Galád, by S. M. Larson & C. W. Hergenrother, and by J. V. Scotti.

Besides the three major condensations A, B, and C, some of the observers reported additional companions, but none of these was detected by more than one group and they all remain unconfirmed. J. V. Scotti (Marsden 1996)

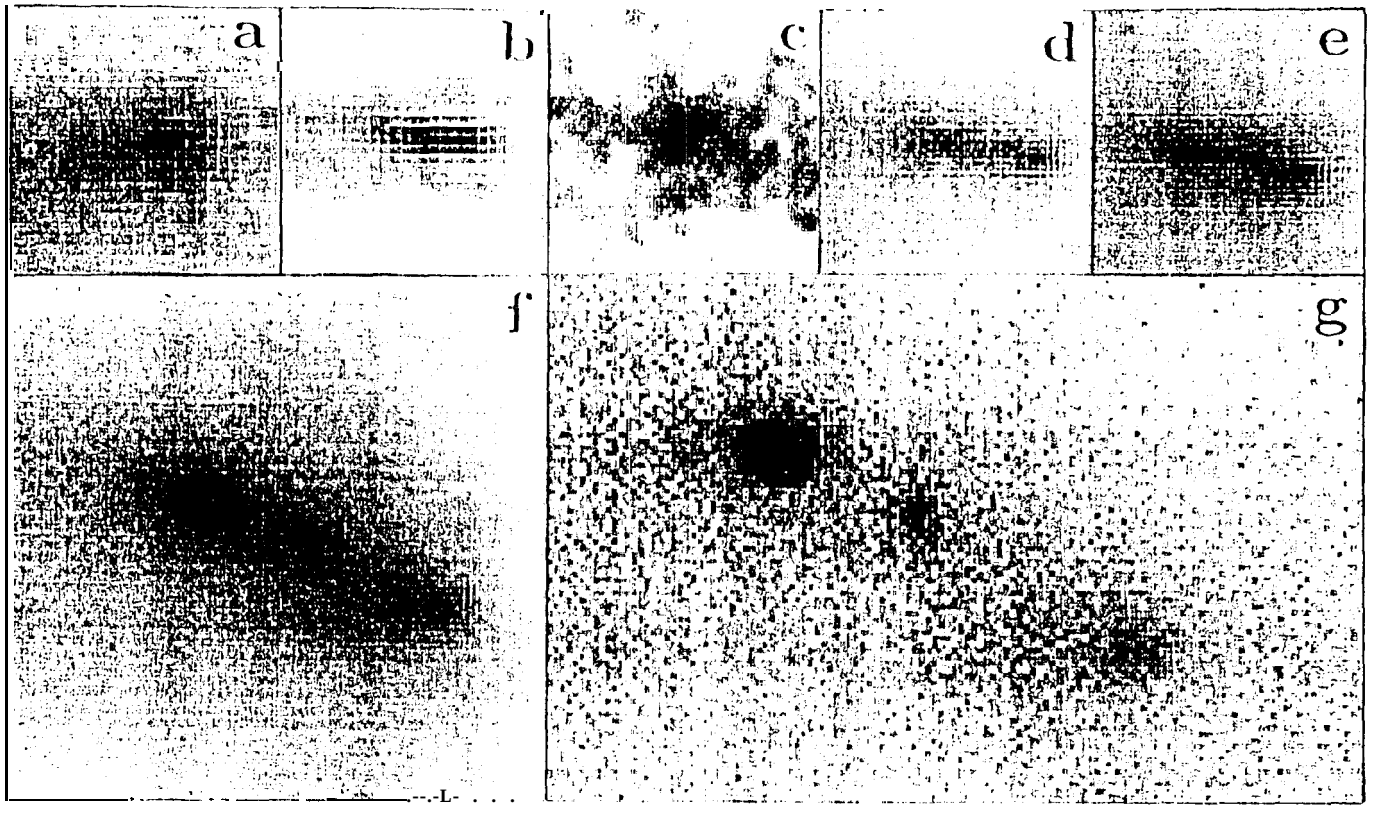

Fig. 2. Examples of high resolution images of P/Schwassmann-Wachmann 3 obtained at ESO La Silla. The individual frames present: (a) a deconvolved version of an image taken by J. Manfroid with the Dutch 0.9-meter reflector on 1995 Oct. 30.032 UT, showing a single condensation; (b) a deconvolved version of an image taken by J. Storm with the Danish 1.5-meter reflector on 1995 Dec. 2.065 UT, showing the condensations A (right) and C; (c) a rebinned infrared image of the condensations A (right), C (left), and F (below C), taken by U. Käufl with the 3.6-meter reflector on 1995 Dec. 12.022 UT; (d) an image of the condensations A (right), B (middle), and C, taken by H. Boehnhardt with the NTT 3.5-meter reflector at the same time the image (c) was taken; (e) an image of the condensations A, B and C (as before), taken by Boehnhardt with the NTT on 1995 Dec. 14.039 UT; (f) an image of the three condensations taken by Käufl with the NTT on 1996 Jan. 7.050 UT; and (g) an image of the condensations taken by Boehnhardt, Käufl & Goudfrooij again with the NTT on 1996 Jan. 31.041 UT. The images have been processed using the ESO's MIDAS software package. The common scale of the images is 0.3 arcsec/mm, so that each of the frames (a) through (c) is 10.8 arcseconds on a side while the dimensions of (p,) are 21.6 by 32.4 arcsec. North is up, east to the left. The position angles of the Sun are 278° on the image (a), 261° on (b), 258° on (c) and (d), 257° on (e), and 254° on (f) and (g).

measured a condensation, called D, less than 2 arcsec to the east-northeast from C on the images taken with the Spacewatch 0.91-meter reflector on Dec. 27. G.J. Garradd (Marsden 1995) reported another condensation, also to the east-northeast of C, some 7 arcsec on Dec. 15 and 8-9 arcsec on Dec. 21, on the images taken with an 0.25-meter reflector at Loomberah, Australia. We refer to this component as E. As mentioned in Sect. 3, the suspected condensation ~2 arcsec to the south of C, detected on the infrared images at ESO on Dec. 12, is referred to as F. Finally, Larson & Hergenrother (Larson 1996) noticed, in another condensation, 3-4 arcsec to the east of the component A, on their images taken with the 2.3-meter reflector of the Kitt Peak National Observatory on Jan. 21, this component is referred to below as G.

5. Modelling relative motions of the components of a split comet

A traditional model for the split comets was based on the assumption that the rate of recession of two fragments is determined entirely by the impulse acquired by them at breakup, that is, by the companion's (initial) velocity of separation from the "principal" nucleus. Application of standard orbit-determination techniques, based on this traditional concept, led repeatedly to disappointing results, as the spatial positions of the respective components, extrapolated back in time, never had even approximately coincided with one another at any instant (e.g., Jeffers 1922, Guigay 1955). It turned out that these difficulties were not a mere product of observational uncer-

Table 1. Overview and summary of measured separations for the fragments A, B, and C from their ESO imaging observations.

Date (UT) of observation	Distance of comet to Earth	Distance of comet to Sun	non-gravitation	A relative to C: Separation (arcsec)	A relative to C: Position angle	B relative to C: Separation (arcsec)	B relative to C: Position angle	Scale (arcsec pixel^{-1})	Telescope; Instrument	Observer(s)
1995 Oct. 28.0410	1.329	1.064		52°				0.40	Danish 1.5-m; DFOSC	Manfroid
30.032°	1.336	1.078		53				0.45	Dutch 0.9-m; CCD	Manfroid
Nov. 28.047[b]	1.553	1.319	57	0.92	277.7			0.24	ESO/MPG 2.2-m; EFOSC2	Reinsch
Dec. 2.(165*	1.599	1.355	58	1.65	270	( )		0.40	Danish 1.5 m; DFOSC	Storm
12.022	1.726	1.448	57	3.80	260.0	2.5	263.0	0.27	NTT 3.5 m; EMMI	Bochnhardt
						(1.45			3.6m; EMMI	Käufl
13.051	1.740	1.458	57	3.81	259.4	2.61	261.6	0.27	ESO/MPG 2.2-m; EFOSC2	Bochnhardt
14.039	1.753	1.467	57	4.24	258.0	2.75	260.8	0.27	NTT 3.5 m; EMMI	Bochnhardt
1996 Jan. 7.050	2.118	1.695	52	10.23	245.5	4.41	250.1	0.27	NTT 3.5-m; EMMI	Käufl
31.041	2.514	1.919	43	17.05	240.5	6.11	244.7	0.27	NTT 3.5-m; EMMI	Bochnhardt[c]

[a] Only a single condensation detected.
[b] Second condensation identified as companion A from dynamical analysis (cf. Sect. 6)
[c] With Käufl and Goudfrooij.

tainties, but had deeper roots: they indicated that the basic premise was incorrect and that the model should fundamentally be revised.

In a series of papers in the late 1970s, a novel model was formulated (Sekanina 1977, 1978, 1979) to interpret the relative motions of fragments of a split comet. In this concept, the rate at which two nuclear components drift apart after their breakup is determined primarily by a minor but detectable difference between the contributions from directed outgassing to the orbital momenta of the two objects. The net effect is thus of the same nature as the nongravitational perturbations of cometary motions. Since the momentum per unit mass transferred from ices sublimating in the general direction of the Sun varies as the inverse characteristic size of each object, the heliocentric motion of a smaller, less massive fragment (companion) is subjected to a continuous deceleration relative to the principal nucleus. The companion is identified by the positive value of this deceleration which is assumed to vary as an inverse square of heliocentric distance and is usually expressed in units of 10^{-5} the solar attraction (1 unit = 5.93×10^{-6} cm/s^2 = 2.96×10^{-9} AU/day^2 at 1 AU from the Sun).

This model has been tested extensively on virtually all comets that are known to have displayed multiple nuclei. The results for the 21 split comets, for which necessary information was available by the early 1980s, were summarized in a review paper by Sekanina (1982). The results for more recent comets with multiple nuclei were reported in several short communications (e.g., Sekanina 1989b, 1995). All these investigations led to a conclusion that projected separation distances between the primary nucleus and a companion could often be satisfied by the model's basic variant, in which case one solves for only two parameters: the time of splitting and the differential radial deceleration of the companion. However, the presence of second-order effects, especially in more extensively observed split comets, has a tendency to weaken the generally high degree of correspondence between observations and the two parameter model. Accordingly, an improved model was introduced in 1978 that allows solutions for up to five parameters, which, in addition to the time of splitting and the deceleration, include three orthogonal components of the separation velocity. Contrary to the traditional approach, however, the separation velocity now contributes only a small fraction of the total effect (up to a few m/s instead of several tens of m/s). The multiparameter model provides an option to solve first for any combination of fewer than the five unknowns, so that a total of 31 different variants of possible solutions are available. This is of vital importance in practice, since the number, the temporal distribution, and the quality of observations dictate the conditions necessary for any particular solution to converge.

6. The multiple nucleus of P/Schwassmann–Wachmann 3 and the sequence of splitting

The analysis of the observed projected separations among the various components was undertaken in two steps. Investigated first were only the extensively observed condensations A, B, and C, of which one is the principal nucleus (the parent object in the first breakup) and two are companions. Objectives were to establish the sequence of splitting (i.e., the order of the breakup events in which the companions came into existence), the circumstances at the times of separation, and the parent bodies. Depending on which of the three components is the parent, numerous breakup scenarios are possible. For example, if C is the parent (as shown below), A could break off from it first

Table 2. Comparison of the parameters and residuals from various solutions for component B separating from C.

Parameter	Solution SD	SND	SRTN	RT ND[a]	SRND	'STN1)	SRTND
Time of splitting t_{split} (days from perihelion)	−24.7 ± 4.9	−20.0 ± 1.1	+16.0 ± 14.9	(-16.0)	−3.2 ± 9.4	+45.8 ± 3.4	+31.7 ± 12.1
(date 1995 UT)	Aug. 29.2	Sept. 2.9	Sept. 28. 9	(S(pt.69)	Sept. 19.7	Nov. 7.7	Oct. 24.6
Separation velocity							
V_{total} (m/s)		(0.114, 0.01)	1.06 ± 0.33	0.24 ± 0.19	(0.46 ± 0.35)	(1.52 ± 0.11	1.07*0.37
V_{radial} (111/S)			+1.05 ± 0.33	−0.11 ± 0.22	+0.45 ± 0.36		+0.43 ± 0.22
V_{transv} (m/s)			+0.09 ± 0.34	−0.18 ± 0.21		-1.51 ± 0.11	−0.97 ± 0.40
V_{normal} (m/s)		+0.11 ± 0.01	+0.11 ± 0.01	+0.11 ± 0.01	+0.11 ± 0.01	+0.13 ± 0.01	+0.11 ± 0.01
Deceleration γ (units of 10^{-5} solar attraction)	2.9 ± 0.4	3.34- 0.1		4.7 ± 1.7	2.7 ± 0.9	18.0 ± 0.8	9.7* 4.2
Mean residual (arcsec)	3.0.329	±0.086	±0.094	±0.085	±0.082	40.072	±0.071

Date U']'	Individual residuals (arcsec) of the 13 employed observations									
	R. A.	Dec.	R.A.	Dec	R.A	Dec	R.A	Dec	R A.	Dec	R.A.	Dec.	R.A.	Dec.
1995 Dec, 12.022	−0.16	+0.41	−0.14	−0.07	0	24	0.04	−0	11	0.0['	0.]7	. 0	05	-0.11	+0.07	−0.12	+0.03
13.051	+ 0.01	+ 0.41	+0.04	-0.07	0	05	0.0'	+0	07	0.06	-1 0.0]	- 0	05	-1 0.06	+0.06	+0.05	+0.02
14.039	− 0.02	+ 0.40	+0.02	- 0.07	0	05	(1,	[1'	+0.05	0.06	0.0(1	0	05	-10.04	+0.04	+0.03	+0.01
23.230	-0.03	+ 0.43	+0.09	+0.01	-1 (1	10	-0.03	+(1.08	-1 0.01	-1 0.09	-} ()	02	-1 0.08	+0.01	+0.08	+0.01
23.234	−0.12	+0.42	0.00	0.00	-1 0	01	-1 0.0,	--0,0]		0.00	0.00	-1 0	01	- (1.02	0.00	−0.01	0.00
24.227	-O.](| I +0.45 | +0.03 | -1 0.04 | -1 0 | 05 | -, 0.0' | -)-(1,02	-1	O.(13	-1 ().03	-} ()	04	-1 0.0)	+0.02	+0.02	+0.03
24.232	-0.09	+0.47	+0.04	-1 0.06	-1 0	06	-, 0.0'	+0.03	-1	0.05	-:0.04	-} 0	06	-10.02	+0.05	+0.03	+0.05
25.213	-0.11	+0.44	+0.02	-1 0.04	-1 0	05	-, 0.0'	-1	0.01	-1 0.03	-1 0.02	-t 0	04	0.00	+0.02	+0.01	+0.02
25.216	0.00	+0.42	+0.13	-1 0.02	-1 0	16	-, 0.0'	+0.12	-1	O.(II	-1 0,)3	-} [1	02	-1 0.11	0.00	+0.12	0.00
27.228	-0.20	+0.26	−0.05	-0,13	- 0	01	- 0.1'	--[1,0';		0.14	0.[14	0	14	- 0.07	−0.17	−0.07	-0.16
27.231	-0.25	+0.32	−0.10	- 0.07	- 0	06	- 0.0'	--0.12		0.08	0.09	- [I.	08	- 0.12	−0.11	−0.11	−0.10
1996 Jan. 7.(I5o	-0.20	+ 0.45	+0.02	+0.13	-1 0	10	-1 0.1)	().(1(	-1	0.12	-1 0.05	-1 0.1)		-1 0.01	+0.02	+0.03	+0.05
31.041	-0.54	+0.29	−0.15	+0.15	- 0	15	- 0.0)	--0.13	+0.16		--0.14	+0.09		0.00	+0.03	-0.03	+0.04

[a] The time of splitting was forced to coincide with the time of onset of the major outburst, t_{split} = 16 days before perihelion

Table 3. Separation parameters of the solutions for the comparisons A, B, D, E, and F relative to C and for G relative to A.

Parameter	B separating from C: Solution I	Solution 1 I	A from C	A from B	D from C	F from C	F from C	G from A
Time of splitting t_{split} (days postperihelion)	31.7 ± 12.1	25.34 10.5	43 9 ± 3.5	72.0 ± 1.7	66 ± 36	61.9 ± 6.0	17	78.6 ± 2.8
(date 1995 UT)	Oct. 24.6	Oct. 18. 2	Nov. 5.8	Dec, 3.9	Nov 28	Nov. 23.8	Oct. 9	Dec. 10.4
Separation velocity								
V_{total} (III/s)	1.07 ± 0.37	1.43 ± 0.20	4 4 1 ± 0.22	4.79 ± 0.32	-	([1 4 ±	0.3)	- -
V_{radial} (111/S)	+0.43 ± 0.22	+ 1.35:1 0.16	4359 ± 0.20	+2.70 ± 0.43	-			
V_{transv} (m/s)	−0.97 ± 0.40	−0.47 ±0.39	2 5 4 ± 0.3 8	- 3.95 ± 0.26	-		-	
V_{normal} (m/s)	+0.11 ± 0.01	+0.10 ± 0.01	,(1) 7 ± (1, [1	−0.10 ± 0.03	-	-1 0 4 ±	0.3	—
Deceleration γ (units of 10^5 solar attraction)	9.7 *4.2	(0.1 ±1.7)	25 0 ± 2.2	343 14	(76 ± 159	367 ± 147	~160	181 ± 14
Number of offset pairs used in the solution	13	15	15	13	2	3	1	2
Mean residual (arcsec)	±0.071	±0.117	± 0.094	,(0.102	±0.26	:10.84	-	±0.15

Table 4. Residuals from the solutions for the component B separating from the primary nucleus C.

Observation date (UT)	Residual o−c (arcsec) from Solution I		Solution II		Observer(s), measurer(s), and observing site
	R.A.	Dec.	R.A.	Dec.	
1995 Nov. 28.047	(+0.81	+0.02)	+0.31	−0.09	Reinsch (ESO)
Dec. 2.065	(+0.34	+0.01)	−0.07	−0.08	Storm (HO)
12,022	−0.12	+0.03	−0.31	0.00	Boehnhardt (ESO)
13.051	+0.05	+0.02	−0.11	−0.01	"
14.039	+0.03	+0.01	−0.01	−0.01	"
23.230	+0.08	+0.01	+0.08	+0.04	Chen, Jewitt (Mauna Kea)
23.234	−0.01	0.00	−0.01	+0.03	"
24.227	+0.02	+0.03	+0.03	+0.06	"
24.232	+0.03	+0.05	+0.04	+0.08	"
25.213	+0.01	+0.02	+0.03	+0.06	"
25.216	+0.12	0.00	+0.14	+0.04	"
27.066	(−.−).36	− 1,06)	(−1.31	0.12)	Scotti (Kitt Peak)
27.071	(−0.93	−0.86)	(−0.89	0.12)	"
27.228	−0.07	−0.16	−0.02	0.12	Chen, Jewitt (Mauna Kea)
27.231	−0.11	−0.10	−0.05	0.06	"
1996 Jan. 7.050	+0.03	+0.05	+0.14	+0.30	Käufl (ESO)

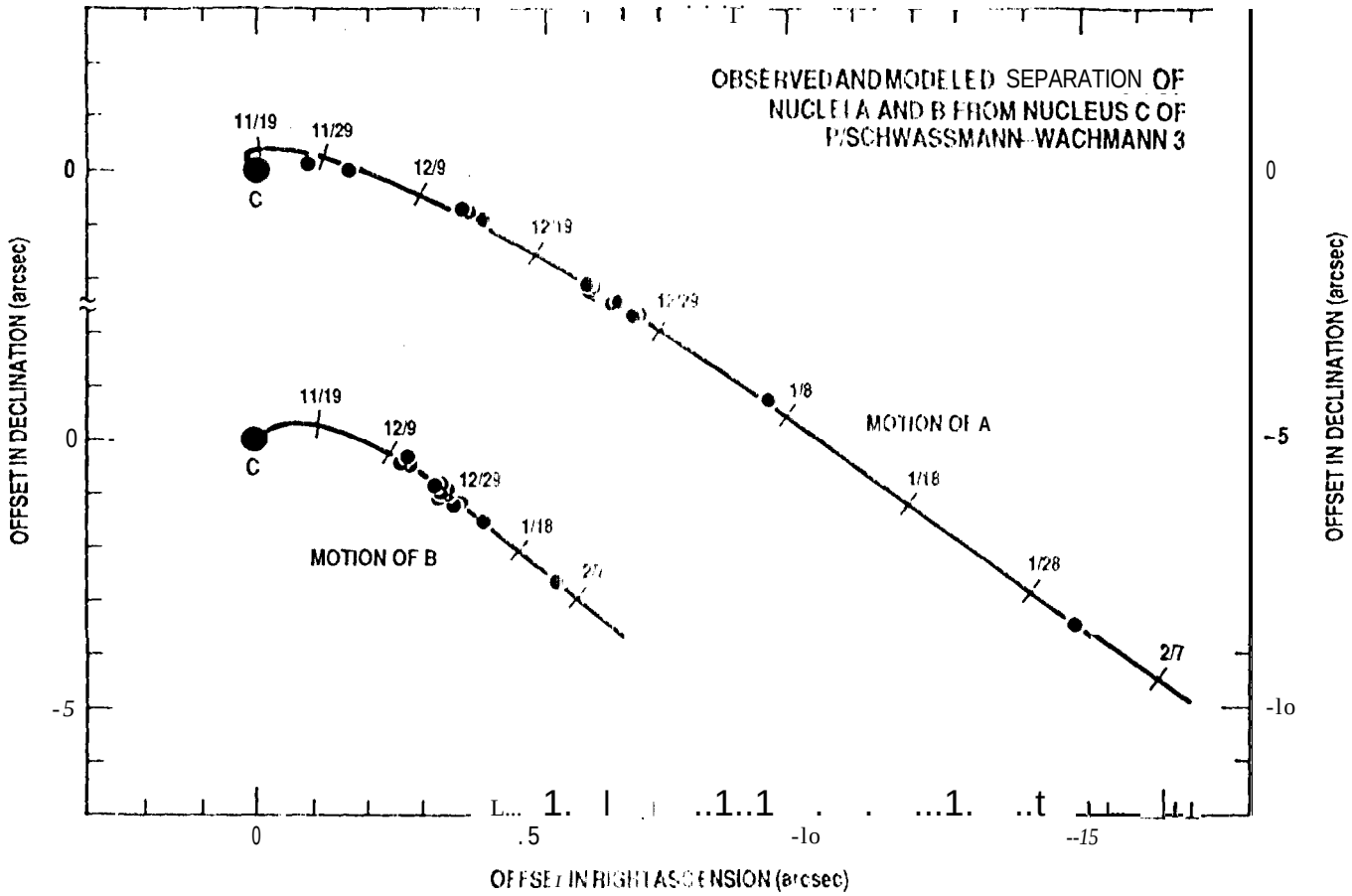

Fig. 3. Models for the motions of the components A and B relative to the primary nucleus C in the time interval from October 1995 till January 1996. The curves represent the dynamical solutions, listed in columns 2 (Solution 1) and 4 of Table 3 for the components B and A, respectively. The tick marks identify the positions of the companions at 0h UT on the indicated dates in late 1995 and early 1996. The dots represent the 15 measured separations of A and the 13 measured separations of B. The scale for the offsets in right ascension is common to the two components. The scale for the offsets in declination is on the right-hand side axis and near the top on the left-hand side axis for A and in the lower part of the left-hand side axis for B.

Components A and C. The results of the preceding subsection indicate that the companion of the Nov. 28 and Dec. 2 images must have been A, in which case it should be possible to link the barely resolved separations of the components on these two images with the other 13 data points to find out whether A broke off from C or B. For either scenario a variety of solutions was again considered and carefully examined, as in the case of B vs. C. The final results for the components A and C are presented in the column 4 of Table 3, with the relevant residuals in the columns 2 and 3 of Table 5. The fit, which is very sensitive to the measured separation on Nov. 28, leaves a slightly larger mean residual than in the case of B vs. C, but all the individual residuals are well within the limit of 0.2 arcsec and show no systematic trends. Considering the difficulties involved in deconvolving the positions of the two detectable components in the images taken in late November and early December (Sect. 3), the measured offsets are in very satisfactory agreement with the predicted separations of A from C: 1.1 arcsec at a position angle of 283° on Nov. 28 and 1.7 arcsec at 272° on Dec. 2. The best fit to the 15 measured separations of A from C is presented in Fig. 3.

Components A and B. The possibility of the component A breaking off from B was initially entertained as the probable scenario (Sekanina 1996), but after the separation distance for the Nov. 28 image had been revised (Sect. 3), this was no longer a viable option. The strongest reason for abandoning this scenario is its unacceptable implication, from the resulting solution in column 5 of Table 3, that the component A did not exist before Dec. 3. Even if the actual uncertainties in the time of splitting are significantly greater than the formal 1σ in Table 3 indicates, the component A would have practically coincided with B in the two early images, which leads to the discrepancies already pointed out above in the case of B vs. C. In addition, the residuals, listed in columns 4 and 5 of Table 5, are on the average larger than for the sce-

Table 5. Residuals from the solutions for the component A separating from C or from B.

Observation date (UT)	Residual $o-c$ (arcsec)			
	A from C		A from B	
	R.A.	Dec.	R.A.	
1995 Nov. 28.047	+0.13	−0.12		
Dec. 2.065	+0.03	−0.06		
12.022	−0.16	+0.08	+0.04	+0.04
13.051	+0.05	+0.14	+0.06	+0.11
14.039	−0.14	+0.07	−0.11	+0.05
23.230	0.00	−0.03	−0.07	−0.06
23.234	−0.02	−0.06	0.00	−0.09
24.227	+0.09	−0.04	+0.09	−0.05
24.232	+0.13	+0.02	+0.12	−0.05
25.213	−0.13	−0.05	−0.12	−0.16
25.216	−0.09	−0.08	−0.20	−0.10
27.228	+0.08	−0.03	+0.15	+0.12
27.231	−0.03	0.00	+0.09	+0.07
1996 Jan. 7.050	+0.10	+0.15	+0.02	+0.09
31.041	−0.02	−0.04	−0.04	+0.03

nario of A breaking off from C and they show a systematic trend (from positive to negative and back to positive) in declination.

Minor components. The solutions for these companions, in columns 6 to 9 of Table 3, are all very crude. Only for the condensation E was it possible to solve for the normal component of the separation velocity in addition to the two basic parameters. In spite of the extremely limited number of positional observations available, the companion G seems the most likely one among the four to be genuine. Even so, only two of its four offset measurements were found to be sufficiently consistent to derive the parameters; the other two left residuals between +0.4 and +1.2 arcsec in either of the two coordinates. The three observations of E are not consistent either, while the deceleration for D is indeterminate. It is probable that the condensation F was a local concentration of small dust particulates with no genuine, sizable fragment involved. If so, the solution for F in Table 3 is meaningless and does not imply the condensation's survival for more than two months, which could not be explained under any plausible circumstances (Sekanina 1982).

7. Relative brightness of the major components

The relative brightness differences among the condensations in the R passband were measured by integrating the flux in a circular aperture of a radius of 2.5 pixels manually centered on the objects. This procedure was repeated similarly to that described for the positional data in Sect. 3. Whenever possible, the results were averaged from sequential exposures taken through the R filter within a time interval of about 30 minutes. The intrinsic variations in the relative brightness of the condensations on a time scale of up to 2 hours and from day to day (Boehnhardt & Käufl 1995) could thus be verified for the NTT observations in December 1995. The estimated uncertainty of the magnitude differences is on the order of 0.03 mag. However, because of the partial overlap of contributions from the neighbouring condensations and also because of the generally uneven level of the background coma intensity around the condensations, an unknown bias may be inherent in our brightness data (especially in the NTT images taken in December 1995).

We also tried to estimate the relative brightness of the condensations on the images of Nov. 28 and Dec. 2, 1995. These efforts were complicated by the fact that on both nights the components could only be separated after applying a deconvolution technique (Sect. 3), whereby the brightness distribution on the images is no longer preserved. Therefore, we tried to assess the relative brightness of the condensations in the original (unprocessed) images in two ways: first, by measuring the maximum flux in a circular aperture centered on the brighter and fainter part of the elongated brightness peak of the coma and, second, by integrating over all pixels in the respective apertures. The values of both methods were averaged for the individual objects. Their uncertainty is much larger than that for the subsequent images described above (on the order of 0.1 mag, compared with 0.03 mag). Nevertheless, it is clear that the brightness difference between the two condensations was well below 0.2 mag.

The magnitude differences between either of the two companions and the principal nucleus C, as derived from the ESO images were combined with the brightness data reported by Galád, by Larson & Hergenrother, and by Scotti (Marsden 1996). The ESO magnitude differences are compared with the other results in Fig. 4, from which it is obvious that the component B was generally fainter than A in the early period, until about the end of 1995. This may explain our failure to detect B on the images of Nov. 28 and Dec. 2. By contrast, the companion B was observed to be mostly brighter than A during January 1996. Thus, even though irregular brightness variations of a few tenths of a magnitude on time scales on the order of hours or less are well documented for both companions in Fig. 4, a fairly well pronounced systematic effect, superimposed on these rapid fluctuations, shows that over the period of two months the component A was fading more rapidly than B. In general, the observed brightness variations of the two companions are similar to those reported for other split comets (Sekanina 1982).

8. The antitail

Inspection of a wide-field image taken with the NTT on Dec. 13, 1995 led to the detection of yet another interesting phenomenon: the dust coma of P/Schwassmann-

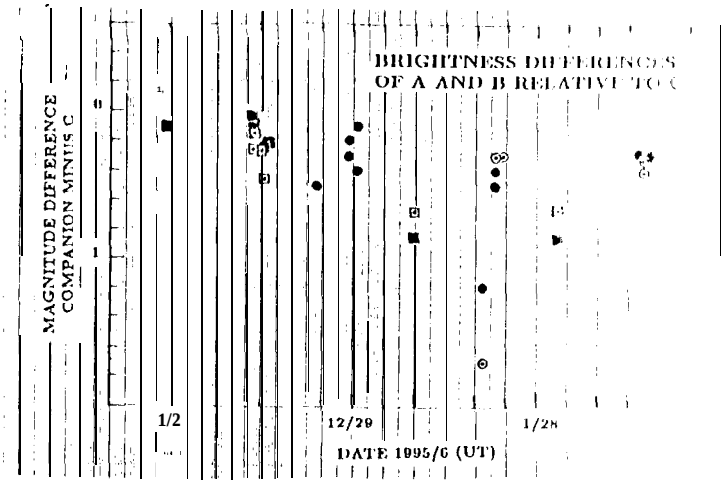

Fig. 4. The magnitude differences between the companions A and B and the principal nucleus C as a function of time. The solid symbols refer to A, the dotted symbols to B. The squares are the various ESO observations, the circles are data published by other observers.

Wachmann 3 was found to be clearly extended in two directions (Boehnhardt & Käufl 1995). In the 8.5 by 8.7 arcmin field, the main tail appeared at a position angle of 80°, nearly coincident with the prolonged radius vector (78°). In addition, a shorter and slightly wider second tail pointed in an approximately sunward direction. Its large-scale appearance can be examined on exposures taken by Jäger (1996) with his 20-cm Schmidt camera. As in the case of any other *antitail*, this feature's sunward orientation is an orbital angular momentum effect on dust particle motions caused by the long-term action of solar radiation pressure and enhanced by favorable projection geometry (e.g., Sekanina 1976a). If such geometry applies, this effect shows especially prominently when Earth transits across the comet's orbital plane, at which time the terrestrial observer views the thin sheet of dust ejecta edgewise. Earth crossed the orbital plane of P/Schwassmann-Wachmann 3 on Dec. 2, 1995 and when the Dec 13 image was taken, the terrestrial observer was only 1°.2 away from the plane as seen from the nucleus. By Jan 7 the angle increased to 30.1 and by Jan. 31 to 3°.9. The major role of the projection effects in the antitail orientation of this comet is indicated by the fact that the angle that the main body of the antitail (which was pointing away from Earth) subtended with the antisolar direction in the comet's orbital plane was only between 40° and 50° in December and January.

The older the dust particles, the greater the angle by which their loci lag, relative to the nucleus, behind the radius vector (i.e., toward the comet's reverse velocity vector). Also, the smaller the particles of a given age, the larger the effect of radiation pressure and the greater their distance from the comet at a given time. Hence very old particles, which are still situated in the proximity of the comet, are necessarily subjected to relatively minor effects of radiation pressure and must therefore be rather large. The particles typically observed in the antitails of comets, including P/Schwassmann-Wachmann 3, are submillimeter- to millimeter-sized.

A dedicated study of this comet's antitail is not undertaken in the framework of this investigation, but is desirable. Here we limit our attention only to cursory inspection of a few images between late October 1995 and the end of January 1996. In Fig. 5 we present examples of the wide-field computer-processed images taken during this period of time at ESO La Sills. The antitail is clearly apparent on the December-January images. The position angle of its maximum extension is measured to have been 250° on Dec. 13, shifting to 240° by Jan. 7 and to 235° by Jan. 31. On the contrary, the October image does not show the antitail at all and the November image displays only its very tenuous traces in a westerly direction.. To understand this evidence and to offer at least an approximate estimate for the age of the ejecta contained in the antitail we summarize, in Table 6, our calculations of the projected orientation pattern for the loci of dust particles ejected at different times.

Table 6. Projected orientation of dust particle loci observed at different times vs. particle ejection time.

Ejection time		Position angle of ejecta loci on images taken in 1995			taken in 1996	
t_{eject} - T (days[a])	Date 1995	Oct. 28	Nov. 28	Dec. 13	Jan. 7	Jan. 31
-200	Mar. 6	289°	264°	255°	247°	243°
-150	Apr. 25	291	264	255	247	243
-100	June 14	293	264	255	246	242
-60	July 24	300	264	255	245	241
-30	Aug. 23	343	265	254	244	240
-16[b]	Sept. 6	64	265	253	243	239
0	Sept. 22	89	272	250	241	238
+15	Oct. 7	95	7:)	227	236	235
+30	Oct 22	98	81	85	220	231
Radius vector[c]		99	82	78	74	74

[a] Reckoned from perihelion: minus sign = before, plus sign = after.
[b] Nominal time of onset of the major outburst.
[c] In projection on to the plane of the sky.

Comparison with the observed position angles on Dec. 13, Jan. 7, and Jan. 31 yields for the dust particles that populated the main body of the antitail an average ejection time of 8±8 days after perihelion, that is, the end of September or the beginning of October 1995. This time coincides with the outburst phase of the light curve in Fig. 1, preceding its peak by about two weeks, and offers further evidence in support of the conclusion that the comet's activity remained elevated for a long period of

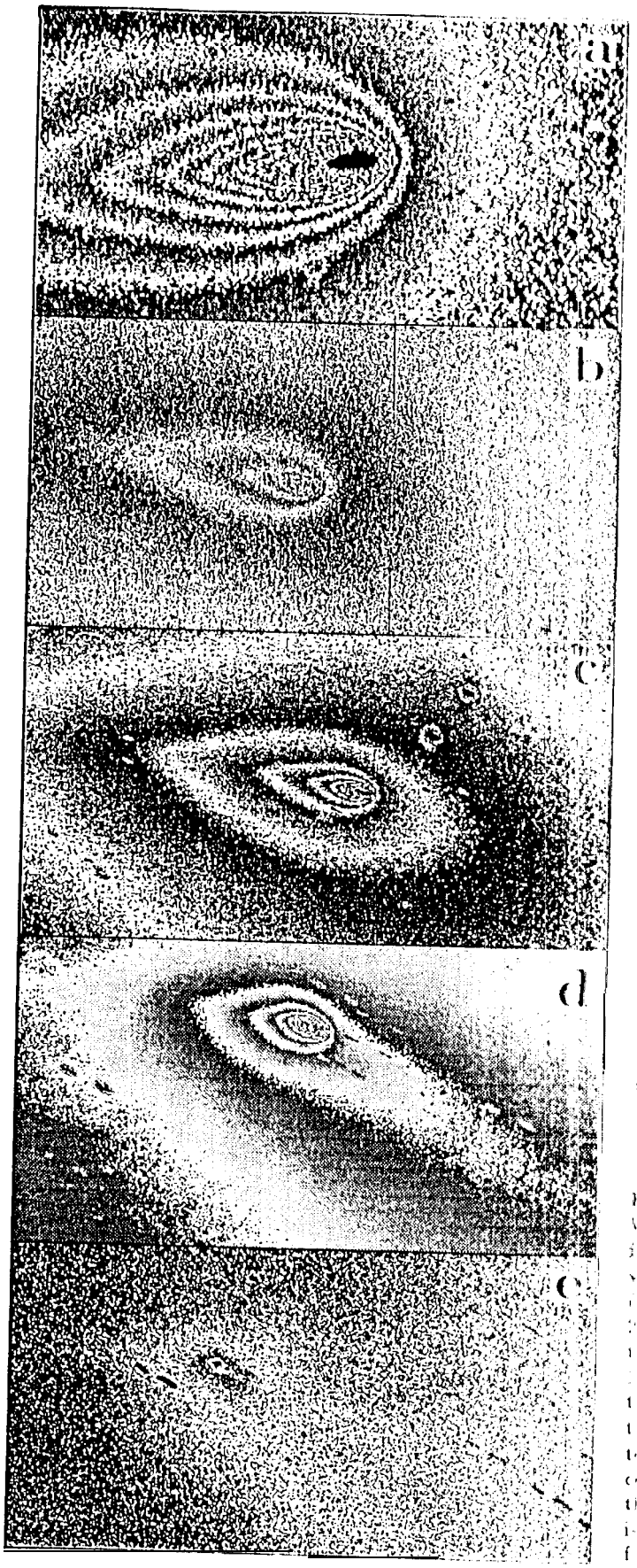

time following the event's onset, at least several weeks, as also documented by other observations. However, by the end of January 1996 the dust production must have decreased dramatically, because the comet shows no longer any ordinary (easterly) tail.

The fact that no obvious antitail shows on the first image in Fig. 5, combined with the distribution of orientations of particle loci in Table 6, signifies a generally lower level of dust production before perihelion and is therefore consistent with the information from the remaining images in the figure. Interestingly, there is no indication on the October image of any excess tail extension in the sector between the position angles of 60° and 90°, which qualitatively suggests that no large amounts of dust in the hundred-micron size range (which would show up in these directions at the relevant distances from the nucleus) were ejected during the first two weeks following the onset of the outburst, even though the comet's brightness was by then already elevated by a few magnitudes. Nevertheless, evidence for preperihelion production of dust is not entirely negative. The results in Table 6 suggest that the elongation of the central condensation at a position angle of ~290°, mentioned in Sect. 3 and clearly evident on the deconvolved image of Oct. 30 in Fig. 2(a), can be interpreted as an integrated effect of the gradual accumulation, over very long periods of time, of fairly large (subcentimeter-sized and perhaps larger) dust particles from early preperihelion emissions. This is an indication that the feature has nothing in common with any secondary condensation in complete agreement with the independent conclusion in Sect. 6.

The images taken near the time of the Earth's transit across the comet's orbital plane are of particular interest. Unfortunately, on the frame from Dec. 2, taken about 12 hours before the transit time, the nucleus is situated near the western edge, making a judgment on the presence of the antitail impossible. On the deconvolved version of this frame's innermost part [Fig. 2(b)], on which the intensity distribution is not preserved, the brightest portion

Fig. 5. Examples of wide-field images of P/Schwassmann-Wachmann 3 obtained at ESO La Silla. The frames present from the top to the bottom: (a) an image taken by J. Manfroid with the Danish 1.5-meter reflector on 1995 Oct. 28.041 UT; (b) an image taken by K. Reinsch with the ESO/MPG 2.2-meter reflector on 1995 Nov. 28.047 UT; (c) an image taken by H. Boehnhardt with the NTT 3.5-meter reflector on 1995 Dec. 13.051 UT; (d) an image taken by H. U. Käufl with the same telescope on 1996 Jan. 7.050 UT; and (e) an image taken by Boehnhardt, Käufl & P. Goudfrooij with the same telescope on 1996 Jan. 31.041 UT. The images have been processed using the ESO's MIDAS software package. The scale of the images is 3.7 arcsec/mm and their width 325 arcsec. North is up, east to the left. The position angles of the Sun are 278° for (a), 262° for (b), 257° for (c), and 254° for (d) and (e).

of the antitail would nearly coincide with the location of the companion condensation and would be largely obliterated. However, very faint traces of the antitail are detectable on the image of Nov. 28, exhibited in Fig. 5(b). Its faintness can in part be explained by the fact that only dust grains expelled before Oct. 2 (9 days after perihelion and earlier) would project to the west of the nucleus in the period of time near the transit (Table 6). This limit virtually coincides with the average ejection time obtained for the main body of the antitail on the subsequent images and implies that particle loci for the ejection times near the critical date of Oct. 2 are greatly foreshortened, complicating their detection. A more definite conclusion would require an extensive investigation of this subject, which is outside the scope of our paper.

9. Outgassing area and the nuclear dimensions

Now that the time line of the elevated activity is established at least qualitatively, we turn our attention to the difficult problem of how large an area of the nucleus surface was involved. Crovisier et al. (1996) find that their peak production rate of hydroxyl nominally implies for the water-production source an outgassing area of ~ 30 km^2, which they find incompatible with the nucleus dimensions derived from Baldet's (1930a,b) nuclear magnitude estimate made during the comet's close approach to Earth in 1930 and point out, correctly in our opinion, that the large inferred sublimation area is a consequence of fragmentation, measuring significant outgassing contributions from ejected icy grains.

While we agree with Crovisier et al.'s (1996) basic interpretation of the effect, our careful analysis of the extent of the outgassing source that is necessary to explain the peak production rate leads to an area somewhat smaller than 30 km^2, as shown below. Although it is virtually certain that the activation of the source proceeded in discrete steps, the steepness of the initial phase of the OH production curve (Fig. 1) suggests that the extended source responsible for the peak emission rate can be modelled as if activated suddenly. To find its outgassing area A that satisfies a total water production rate Q, we consider the source to be centered on the subsolar point and its radial extent on the spherical nucleus, of a diameter D, to be limited by the Sun's zenith angle $z_{\rm lim}$. Then

$$A = \tfrac{1}{2}\pi D^2 (1 - \cos z_{\rm lim}). \qquad (1)$$

A simple model of water sublimation from point sources on a cometary nucleus, which accounts for the variations in the rate of outgassing with distance from the subsolar point and which is based on the assumed energy balance between the insolation on the one hand and pure water sublimation and thermal reradiation on the other, was formulated by Sekanina (1988). This model is here generalized to an extended source of any size smaller than the area of the sunlit side of the nuclear surface. The model offers an expression for the sublimation rate per unit area, $Z_0(r)$, at the subsolar point at a heliocentric distance r (at an assumed albedo of 0.04 and emissivity of unity) and allows one to calculate the sublimation rate per unit area $Z(z, r)$ at the Sun's zenith angle z in terms of $Z_0(r)$:

$$Z(z,r) = Z_0(r) \cdot \zeta(z,r), \qquad (2)$$

where

$$\zeta(z,r) = \cos z - f(r) \sin^2 z \quad \text{for } 0 \le z \le z_{\rm crit}, \qquad = 0 \quad \text{for } z > z_{\rm crit}, \qquad (3)$$

where $f(r)$ is a function of heliocentric distance only. The approximation for large zenith angles is of no consequence in practice. For $r \ll 3$ AU, $z_{\rm crit}$ is only slightly smaller than 90°. The water sublimation rate per unit area averaged over the entire source is then

$$\langle Z \rangle = \frac{1}{\cos z_{\rm lim}} \frac{Z_0}{} \int_0^{z_{\rm lim}} \zeta(z,r) \sin z \, dz = Z_0 \left[\left(\tfrac{1}{2} - \tfrac{2}{3} f \right) + \left(\tfrac{1}{2} + \tfrac{1}{3} f \right) \cos z_{\rm lim} + \tfrac{1}{3} f \cos^2 z_{\rm lim} \right] \qquad (4)$$

Since the production rate of water from the source is $Q = \langle Z \rangle A$, the expression (4) can be rewritten, with the help of (1), as follows

$$\frac{12Q}{\pi Z_0 D^2} = 3 - 4f + 6f \cos z_{\rm lim} - 3\cos^2 z_{\rm lim} + 2f \cos^3 z_{\rm lim}. \qquad (5)$$

For a given production rate Q at a heliocentric distance r (which defines Z_0 and f), this cubic equation in $\cos z_{\rm lim}$ yields only one physically meaningful root, which is a function of the nuclear diameter D

$$\cos z_{\rm lim} = \frac{1}{f} \left[\sqrt{1 + 4f^2} \cos \tfrac{1}{3}(\pi - \theta) - \tfrac{1}{2} \right], \qquad (6)$$

where

$$\theta = \arccos \left[\frac{1 + 4f^2 (C + 2f)}{(1 + 4f^2)^{3/2}} \right] \qquad (7)$$

and

$$C = \frac{6Q}{\pi Z_0 D^2}. \qquad (8)$$

The outgassing area A then results from (1) with $\cos z_{\rm lim}$ from (6). The minimum nuclear diameter $D_{\rm min}$ that satisfies a particular value of the production rate $Q(r)$ at a heliocentric distance r is calculated from (5) after $z_{\rm lim}$ has been replaced with $z_{\rm crit}$.

This model was applied to the peak production rate of water from P/Schwassmann Wachmann 3, which was assumed to be equal to the peak OH production rate of $Q = 22.2 \times 10^{28}$ H$_2$O/s, as measured by Crovisier et al. (1996). The results are presented in Table 7. The smallest effective nuclear diameter that is compatible with the entire observed outgassing area being due to the emission

Table 7. Nuclear diameters, averaged water sublimation rates per unit area, outgassing areas of activated source, and limiting zenith distances of the Sun that satisfy the water production rate of 22.2×10^{28} mol/s at a heliocentric distance of 0.95 AU.

Effective nucleus diameter, D (km)	Sublimation rate per unit surface area, $\langle Z \rangle$ (10^{28} mol/km^2/s)	Outgassing area of the activated source, A (km^2)	Fraction of nuclear surface active (percent)	Limiting zenith angle of the Sun z_{lim}
4.2[a]	0.84	26.5	48[b]	88°
4.5	1.15	19.3	30	67°
5.0	1.30	17.0	22	56°
6.0	1.45	15.3	14	43°
8.0	1.57	14.2	7	31°
10.0	1.62	13.7	4	24°

[a] Minimum allowed effective diameter D_{min} of the nucleus
[b] The entire sunlit hemisphere; the fraction is less than 50 percent because of the employed approximation at $z \simeq 90°$ in Eq (3)

source on the nucleus surface (and not, in part, to a cloud of ejected icy grains) is 4.2 km, in which case the sudden activation would have involved the whole sunlit hemisphere, a very unlikely case. A more realistic scenario, with less than ~20 percent of the surface involved, requires that the nucleus be more than 5 km across.

This estimate does not compare favorably with limited photometric evidence. As interpreted by Sekanina (1989a), Baldet's (1930a,b) visual observation made with the 83-cm refractor at Meudon at the time of close approach to Earth in 1930 implies an effective nuclear diameter about five times as large as Baldet's result of 0.4 km, when one uses a modern value of 4 percent for the geometric albedo and when one corrects for the solar phase effect, which, although very significant, was neglected by Baldet altogether. On the other hand, quasispecular reflection from isolated, relatively bright, multifaceted specks of $<<1$ km^2 on the nucleus could also account for the star-like object detected by Baldet (Sekanina 1989a), with the much darker bulk of the nuclear surface having remained unrecognized by him on account of a low contrast. In the light of these uncertainties it is remarkable that the comet's brightness at the time of its recovery in late 1994 (Birkle et al. 1994) implies, as seen from Table 8, an effective nuclear diameter that is virtually identical with the value derived by straightforwardly interpreting Baldet's magnitude estimate as referring to the entire nucleus. The agreement is perfect when one uses a value of 0.035 mag/deg for the coefficient of the solar phase law. The employed assumptions on the geometric albedo p and the phase slope β are based on the results of recent nucleus investigations of 1P/Halley and a few periodic comets of low activity, such as 2P/Encke, 7P/Pons-Winnecke, 10P/Tempel 2, 28P/Neujmin 1, 49P/Arend-Rigaux and C/1983 H1 IRAS-Araki-Alcock (e.g., Sekanina 1989a, 1991, Hanner et al. 1985, Tokunaga & Hanner 1985, Brooke & Knacke 1986, Delamere et al. 1986, Sagdeev et al. 1986, Birkett et al. 1987, Campins et al. 1987, Jewitt & Meech 1987, 1988, Veeder et al. 1987, Millis et al. 1988, A'Hearn et al. 1989).

The results from Birkle et al.'s 1994 and Baldet's observations are seen from Table 8 to be in excellent agreement. In addition, the implied nuclear dimensions are consistently and rather tightly constrained by the observations from March 1995. The 1994 data points are the most relevant, in part because of their high quality, in part because of their relative insensitivity to errors in the solar phase law. Even if P/Schwassmann-Wachmann 3 should have had one of the darkest cometary nuclei, with a very steep slope of its phase curve, it still could not have been more than 5 km across before the recent splitting, the best guess being some 2–3 km. This result points conclusively to the presence in the coma of an extended source of freshly ejected icy grains, which contributed significantly to the water production rate peaking in the early stages of the comet's outburst.

10. Final comments and conclusions

The firm conclusion to which our investigation lends support is the identification of the component C with the principal nucleus in which most of the mass of the original comet is contained. Dismissing the solution for the companion 1 (column 8 of Table 3) as too uncertain to take seriously, the earliest breakup event involved the companion B, which split off most probably in late October 1995, with a 1σ uncertainty of nearly two weeks. This event was followed closely by a secondary breakup, in early November 1995, in which the parent C gave birth to the companion A. It even is possible that both companions broke off from C simultaneously. The suspected companions D and E, if genuine, separated from C most probably in late November, while G is likely to have split off from A in early December. The derived differential decelerations imply that B should be the most massive companion and there is a chance that it still will be observable after the comet emerges, in June 1996, from the conjunction with the Sun. The apparently less massive companion A, may be a much more difficult target later in 1996 and its detection, if possible at all, may require use of the Hubble Space Telescope. If continuing, the pronounced rate of brightness decrease of A (Sect. 7) would support the conclusion that A was less massive than B. The derived separation velocities, 1.1 m/s for B and 4.4 m/s for A, further underscore the differences between the two fragments. None of the four suspected companions D–G, with their high decelerations, could be a substantial piece of material (more than, say, several tens of meters across) and the indications are that each of them disintegrated shortly after separating from the parent body. We are rather confident that F, which was undetected in the optical region of the spec-

Table 8. Effective nuclear diameters from comparison of brightness observations made under diverse geometric conditions.

Observation date (UT)	Distance (AU) of comet to Earth	Distance (AU) of comet to Sun	Phase angle	Observed magnitude (visual, V, or $R_{C,Cous}$)	Reference	Effective nuclear diameter[a] (km) β = 0.035 mag/deg, p = 0.04	β = 0.035 mag/deg, p = 0.02	β = 0.050 mag/deg, p = 0.04	β = 0.050 mag/deg, p = 0.02
1930 May 30.048[b]	0.063	1.033	70°.3	14 (vis.)	Baldet (1930a,b)	2.3	3.2	3.7	5.2
1994 Dec. 28.076[c,d]	2.362	3.034	15.4	22.2 (V)	this paper[e]	2.3	3.2	2.5	3.5
28.194[c,f]	2.360	3.033	15.4	22.1 (V)	this paper				
29.052[g]	2.344	3.027	15.3	22.2 (V)	this paper				
29.140[c,h]	2.343	3.027	15.3	22.1 (V)	this paper				
1995 Mar. 28.060[i]	1.678	2.348	21.5	19.8 (R)	this paper	<3.5	<4.9	<4.0	<5.7
29.076[i]	1.681	2.340	21.8	19.7 (R)	this paper	<3.6	<5.1	<4.2	<6.0
June 25.973[j]	1.871	1.532	32.9	16.6 (R)	this paper	...	...	...	...

[a] Assumed photometric parameters are phase coefficient β and geometric albedo p in the V passband.
Assumed $V - m_{vis} = -0.12$ mag.
[c] This image was taken with the 3.5-meter reflector at Calar Alto, only marginal signal contribution from the coma.
[d] This image and an image taken through a red filter on 28.053 yield $(V - R)_{Johnson} = +0.70$ mag.
[e] Preliminary magnitude published by Birkle et al. (1994).
[f] This image and an image taken through a red filter on 28.178 yield $(V - R)_{Johnson} = +0.59$ mag.
[g] This image and an image taken through a red filter on 29.055 yield $(V - R)_{Johnson} = +0.45$ mag.
[h] This image and an image taken through a red filter on 29.128 yield $(V - R)_{Johnson} = +0.38$ mag.
[i] This image was taken with the Danish 1.5-meter reflector at ESO La Silla; assumed $(V - R)_{Cousins} = +0.36$ mag; developing coma.
[j] This image was taken with the ESO/MPG 2.2-meter reflector at ESO La Silla; assumed $(V - R)_{Cousins} = +0.36$ mag; strong coma already developed, no meaningful constraints on the nuclear size possible.

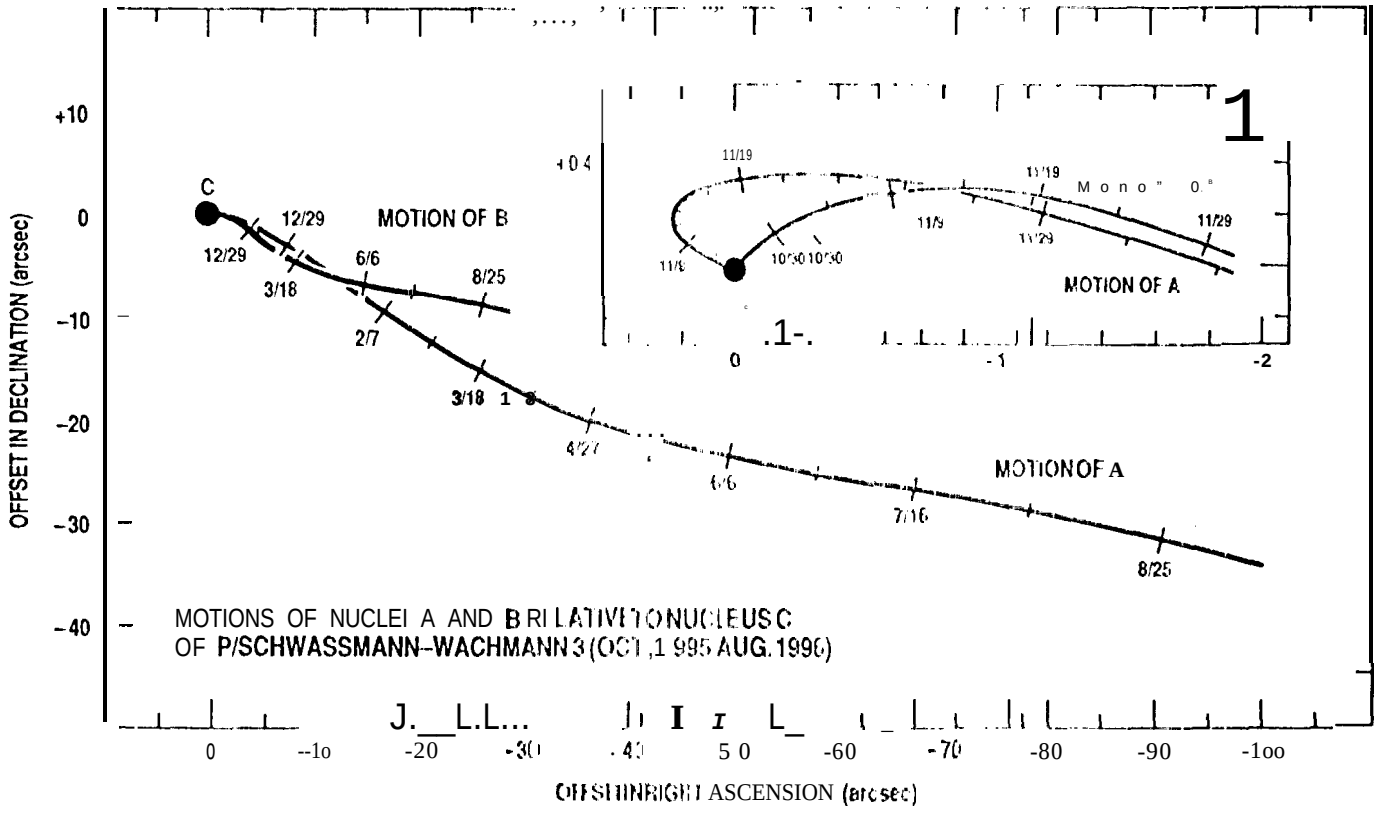

Fig. 6. Predicted motions of the companions A and B relative to the principal nucleus C, based on the dynamical solutions listed, respectively, in columns 2 and 4 of Table 3. The tick marks identify the positions of the companions at 0h UT on the indicated dates in December 1995 and in 1996. The insets show the predicted motions in the early period, before the multiple nucleus was discovered. Note that the inset scale is enlarged by a factor of 25.

trum, was not a companion in the true sense of the word (i.e., dominated by a single discrete mass).

To illustrate the future expected dynamical evolution of the system of the three major condensations, we present the ephemerides for the components A and B relative to C in Fig. 6 up to the end of August 1996. It is predicted that, after the comet emerges from the conjunction with the Sun, the three condensations (if all still detectable) will continue to be closely aligned along a straight line at a position angle of ~250°, the separatism distances increasing gradually from 60 arcsec in late June to 100 arcsec in late August. for the component A arid from 18 arcsec to 28 arcsec for B in the same period of time In the inset of Fig. 6 we plot the calculated motions of the two companions with respect to the principal component C in the early period, before the discovery of the multiple nucleus. The configuration of the three condensations varied significantly during this interval of time and if the proximity of the components and the extreme faintness of B did not prevent us from imaging the group, we would have witnessed a sequence of rapidly changing positional patterns during November, as depicted schematically in Fig. 7.

The issue of particular interest is the relationship between the outburst and the breakup events. Even though the time of separation of B from C, nominally the earliest breakup episode, is, realistically, uncertain to at least ±2 weeks, an attempt to force the time of this breakup to coincide with the onset time of the major outburst in early September led to a solution (RTND in column 5 of Table 3) that was unsatisfactory, leaving for the two critical January observations systematic residuals in declination that were well in excess of 0.1 arcsec, exceeding the *maximum* expected error by a factor of several, and amounting to about three times the residuals from the accepted solution SRTND. These residuals were deemed large enough not to consider the corresponding forced solution to be equivalent to the formally best fit. On the other hand, the solution STND (column 7 of Table 3), which for all practical purposes was as good as the solution SRTND, yielded for the separation time an even later date, nearly coinciding with the separation time of the component A, increasing the time difference between the outburst and the splitting from six weeks to two months.

The derived times of separation for the companions B and A from C correlate well with two less prominent secondary flare-ups on the light curve. The nominal times for the two major nuclear fragmentation events, 32 and 44 days postperihelion, precede the sharp peaks of these flare-ups by 4-5 days, virtually coinciding with their onset times.

The final issues that we wish to address, those of the probable physical nature of the companion nuclei, the process resulting in their birth, and the trigger, necessarily involve speculative considerations. Analysis of differential nongravitational decelerations led to the conclusion that the companion nuclei of nontidally split comets may

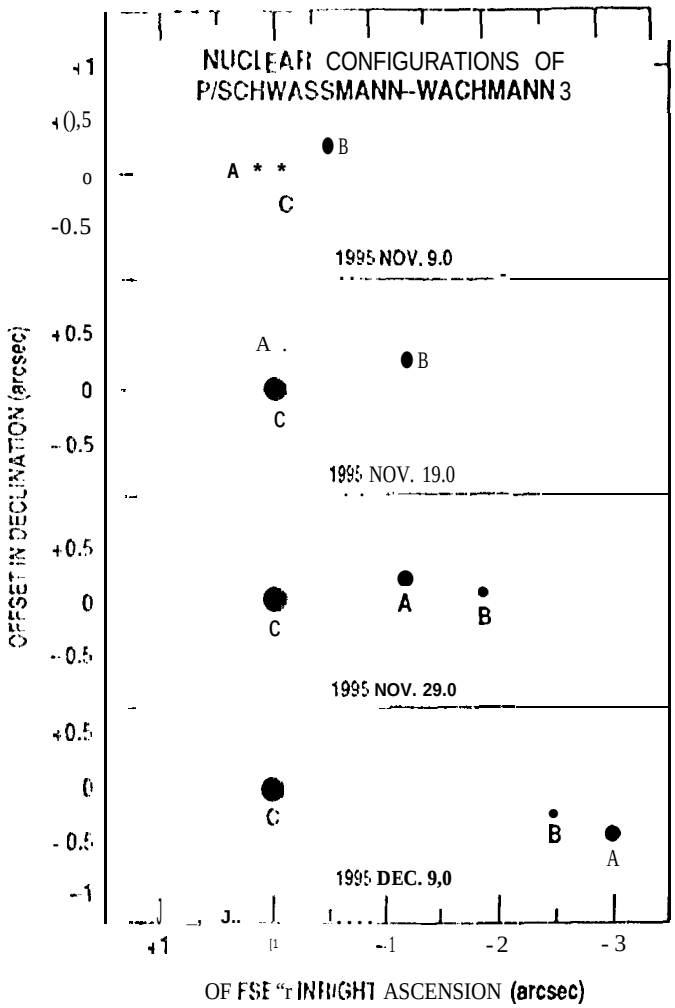

Fig. 7. Changing configuration of the condensations A, B, and C during November and early December 1995, as derived from their modeled relative motions. Note that in early December, A and B exchanged their positions relative to C and that B was the westernmost component until Dec. 5. Similarly, the main condensation C was the southernmost of the three until Dec. 2, but the northernmost from Dec. 3 on. The times are UT.

represent subkilometer-sized, pancake-shaped, nearly inert fragments of the surface mantle detached from the rest of the nucleus (Sekanina 1982). The idea of a buildup of an insulating dust mantle, first expressed by Whipple (1950) as an attribute of his dirty-ice conglomerate model nucleus, has been increasingly popular in the past quarter of the century (e.g., Dobrovolskij & Markovich 1372, Mendis & Brin 1977, Brin & Mendis 1979, Brin 1980, Horanyi et al. 1984, Janaki & Salvail 1984, Podolak & Herman 1985, Rickman & Fernandez 1986 and Rickman et al. 1990). The problem with the early versions of the concept was the prediction of the mantle's blowoff at heliocentric distances near 1 AU, contradicted by imaging evidence from the Halley missions (e.g., Keller et al. 1987). An important re-

vision of the icy-conglomerate model and the dust-mantle concepts was Keller's (1989) suggestion that cometary nuclei resemble icy dirtballs rather than dirty snowballs. Also supported by high refractory-to-volatile mass ratios (≥ 1), inferred from independent lines of evidence (McDonnell et al. 1991, Sykes & Walker 1992), Keller's argument has fundamentally shifted the emphasis from the volatile fraction to the refractory component and, together with the major results from recent laboratory comet-simulation experiments (Grün et al. 1991), opened avenues for innovative investigations of the physical processes that take place on cometary nuclei.

Very recently, Kührt & Keller (1994) introduced the concept of an inert, porous, but cohesive *crust*, to be distinguished from the various concepts of a strengthless *mantle* supported against the vapor pressure only by self-gravity. A typical strength of the crust matrix, including its interface with the underlying layer of dust-ice mix (but also dominated by the refractory component), is estimated by Kührt & Keller at 1 mbar to 1 bar, sufficient to protect it from disruption by the vapor pressure. To account for activity from small, isolated sources, they resort in an extension of the model advocated by Donn (1990) to the inevitable presence of large-scale compositional inhomogeneities, with macroscopic fractal clusters of refractory matrix (as opposed to icy material) dominating much, but not the entirety, of the nucleus surface layer. They also consider other potential triggers of localized activity, including thermal stresses.

Another scenario, also derived from Kührt & Keller's (1994) concept of a cohesive crust, was developed by Möhlmann (1996), who proposed that pressure driven lateral subsurface flows of liquid water are occasionally possible in such a porous cohesive crust. While the possible existence of subsurface water "lakes" in cometary nuclei was considered before (Wallis 1986), Möhlmann's argument is based on a potentially important property of the temperature and pressure distributions through the interior of the crust at heliocentric distances near 1 AU if the temperatures vary from ~400 K at the surface to ~200 K at the interface with the core and if the pressures vary from near zero at the surface to as much as 10 mbar at the interface (requiring, though, a high thermal conductivity), then a layer may exist in the crust, where the temperature is near 273 K and the pressure near 0.0061 bar, which define the triple point of water. It is likely that processes involving liquid water (such as its lateral flow or refreezing, accompanied by an inevitable expansion) could significantly damage the structural integrity of the crust, perhaps to the point of inflicting major cracks or even fracture. While it remains to be seen whether Möhlmann's scenario is plausible, the recent research on cometary nuclei appears to be headed in the direction of an ever increasing depth of the inert surface layer; some of these scenarios considered by Kührt & Keller (1994) yield crusts more than 5 meters thick. It is informative to compare these modeled crust depths with an estimated thickness of the pancake-shaped companion fragments calculated by Sekanina (1982) from their differential decelerations: for the group of the most rapidly disintegrating companions, with a characteristic deceleration of $\gamma \simeq 300$ units of 10^{-5} solar attraction and a typical lifetime of ~20 days at 1 AU from the Sun, the minimum dimension inferred was ~7 meters; for larger companions, whose $\gamma \simeq 40$ units and lifetime ~50 days, the minimum dimension required was ~50 meters. It seems that given the apparently very heterogeneous interior structure of a cometary nucleus in general and its cohesive crust in particular, the proposed relationship between large fragments of the crust on the one hand and at least some among the secondary nuclei of nontidally split comets remains a plausible hypothesis. The triggers that activate a discrete source should also be responsible for fracture. The delayed response of the nucleus of P/Schwassmann-Wachmann 3 to a major disturbance on its surface, reflected in the enormous time difference between the onset of the major outburst and the subsequent breakup events, clearly supports the conceptual interpretation of a cometary nucleus as an object that possesses a limited, but not insignificant, internal cohesion. The effect also provides strong evidence against models of a strengthless cometary nucleus.

Acknowledgements. We thank J. Manfroid (University of Liège, Belgium), K. Reinsch (University of Göttingen, Germany), and J. Storm (ESO, La Silla, Chile) for kindly making available to us their images of the comet from, respectively, Oct. 27.29, Nov. 28, and Dec. 2. We also thank T. Goudfrooij (ESO, Garching, Germany) for allowing us to use his NTT observing time and C. W. Hergenrother, S. M. Larson, B. G. Marsden, and J. V. Scotti for their communications. Our observing profited greatly from the professional assistance by the ESO staff members G. Martin, J. Miranda, and H. Nunez. This research was carried out in part by the Jet Propulsion Laboratory, California Institute of Technology, under contract with the National Aeronautics and Space Administration.

References

A'Hearn, M. F., Campins, H., Schleicher, D. G. & Millis, R. L. 1989, ApJ 347, 1155
Baldet, F. 1930a, Compt. Rend. Paris 190, 1382
Baldet, F. 1930b, Bull. Soc. Astron. France 44, 433
Belyaev, N. A. & Shaporev, S. D. 1975, Probl. Cosmic Phys. 10, 9 (in Russian)
Birkett, C. M., Green, S. F., Zarnecki, J. C. & Russell, K. S. 1987, MNRAS 225, 285
Birkle, K., Boehnhardt, H. & Schwehm, G. 1994, IAU Circ. No. 6122
Boehnhardt, H. & Käufl, H. U. 1995, IAU Circ. No. 6274
Boehnhardt, H., Käufl, H. U., Goudfrooij, P., Storm, J., Manfroid, J. & Reinsch, K. 1996, ESO Messenger, submitted
Brin, G. D. 1980, ApJ 237, 265

Brin, G.D. & Mendis, D. A. 1979, ApJ 229, 402
Brooke, T. Y. & Knacke, R.F. 1986, Icarus 67, 80
Campins, H., A'Hearn, M. F. & McFadden, L. A. 1987, ApJ 316, 847
Chen, J., Jewitt, D. 1994, Icarus 108, 265
Crovisier, J., Biver, N., Bockelée-Morvan, D., Colom, P., Gérard, E., Jorda, L. & Rauer, H. 1995, IAU Circ. No. 6227
Crovisier, J., Bockelée Morvan, D., Gérard, E., Rauer, H., Biver, N., Colom, P. & Jorda, L. 1996, A&A, submitted
Delamere, W. A., Reitsema, H. J., Huebner, W. F., Schmidt, H.U., Keller, H. U., Schmidt, W. K. H., Wilhelm, K. & Whipple, F. L. 1986, in: B. Battrick, E. J. Rolfe & R. Reinhard (eds.), Exploration of Halley's Comet, ESA SP 250, ESTEC, Noordwijk, vol. 2, p. 355
Dobrovolskij, O. V. & Markovich, M. Z. 1972, in: G. A. Chebotarev, E. I. Kazimirchak-Polonskaya & B. G. Marsden (eds.), The Motion, Evolutions of Orbits and Origins of Comets, Reidel, Dordrecht, p. 287
Donn, B.D. 1990, A&A 235, 441
Fanale, F. P. & Salvail, J. R. 1984, Icarus 60, 476
Feijth, H. 1980, Internat. Comet Quart. 2, 73
Fernie, J. D. 1983, PASP 95, 782
Green, D. W. E., (cd.) 1980, Internat. Comet Quart. 2, 1
Green, D. W. E., (cd.) 1981, Internat. Comet Quart. 3, 21
Green, D. W. E., (rd.) 1990, Internat. Comet Quart. 12, 66, 67, 102, 103, 163
Green, D. W. E., (cd.) 1991, Internat. Comet Quart. 13, 59, 81, 165
Green, D. W. E., (rd.) 1992, Internat. Comet Quart. 14, 73
Green, D. W. E., (cd.) 1993, Internat. Comet Quart. 15, 79
Green, D. W. E., (rd.) 1995a, Internat. Comet Quart. 17, 192
Green, D. W. E., (cd.) 1995b, Internat. Comet Quart. 17, 210, 211
Green, D. W. E., (rd.) 1996, Internat. Comet Quart. 18, 43
Grün, E., Bar-Nun, A., Benkhoff, J., Bischoff, A., Dorschner, J., Hellmann, H., Hesselbarth, P., Hsiung, P., Keller, H. U., Klinger, J., Knölker, J., Kochan, H., Kohl, H., Kölzer, G., Kramkowsky, D., Lämmerzahl, P., Mauersberger, K., Neukum, G., Oehler, A., Ratke, L., Roessler, K., Spohn, T., Stöffler, D. & Thiel, K. 1991, in: R. L. Newburn, Jr., M. Neugebauer & J. Rahe (eds.), Comets in the Post-Halley Era, Kluwer, Dordrecht, p. 277
Guigay, G. 1955, J. Obs. 38, 189
Hanner, M. S., Aitken, D. K., Knacke, R., McCorkle, S., Robert, P. F. & Tokunaga, A. T. 1985, Icarus 62, 97
Herald, D. 1979, Minor Planet Circ. No. 5(I24
Horanyi, M., Gombosi, T. I., Cravens, T. E., Körösmezey, A., Kecskeméty, K., Nagy, A. I. & Szegö, K. 1984, ApJ 277, 449
Howarth, I. D. & Bailey, J. 1980, J. Brit. Astron. Assoc. 90, 265
Jäger, M. 1996, Sterne und Weltraum 4/96, 291
Jeffers, H. M. 1922, Lick Obs. Bull. 10, 120
Jewitt, D. & Meech, K. J. 1986, ApJ 310, 937
Jewitt, D. & Meech, K. J. 1987, AJ 93, 1542
Jewitt, D. C. & Meech, K. J. 1988, ApJ 328, 974
Johnson, H. L. 1955, Ann. d'Astrophys. 18, 292
Keller, H. U. 1989, in: J. Hunt & T. D. Guyenne (eds.), Physics and Mechanics of Cometary Materials, ESA SP 302, ESTEC, Noordwijk, p. 39
Keller, H. U., Delamere, W. A., Huebner, W. F., Reitsema, H. J., Schmidt, H.U., Whipple, F. L., Wilhelm, K., Curdt, W., Kramm, R., Thomas, N., Arpigny, C., Barbieri, C., Bonnet, R.M., Cazes, S., Coradini, M., Cosmovici, C. B., Hughes, D. W., Jamar, C., Malaise, D., Schmidt, K., Schmidt, W. K. H. & Seige, P. 1987, A&A 187, 807
Kron, G. E. & Mayall, N. U. 1960, AJ 65, 581
Kührt, E. & Keller, H. U. 1994, Icarus 109, 121
Landgraf, W. 1983, Sterne 59, 153
Landolt, A. U. 1992, AJ 104, 340
Larson, S. M. 1996, personal communication
Lucy, L. B. 1974, AJ 79, 745
Marsden, B. G. 1995, personal communication
Marsden, B. G., (cd.) 1996, Minor Planet Circ. Nos. 26211, 26444 5, 26599, 26(,1(1 1
McDonnell, J. A. M., Lamy, P. L. & Pankiewicz, G. S. 1991, in: R. L. Newburn, Jr., M. Neugebauer & J. Rahe (eds.), Comets in the Post-Halley Era, Kluwer, Dordrecht, p. 1043
Mendis, D. A. & Brin, G. D. 1977, Moon Planets 17, 359
Millis, R. L., A'Hearn, M. F. & Campins, H. 1988, ApJ 324, 1194
Möhlmann, D. 1996, Planet. Space Sci., submitted
Podolak, M. & Herman, G. 1985, Icarus 61, 267
Richardson, W. H. 1971, J. Opt. Soc. Am. 62, 55
Rickman, H. & Fernández, J. A. 1986, in: O. Melita (cd.), Comet Nucleus Sample Return Mission, ESA SP- 249, ESTEC, Noordwijk, p. 185
Rickman, H., Fernández, J. A. & Gustafson, B. Å. S. 1990, A&A 237, 5.14
Sagdeev, R. Z., Avanesov, G. A., Ziman, Ya. I., Moroz, V. I., Tarnopolsky, V. I., Zhukov, B. S., Shamis, V. A., Smith, B. & Toth, I. 1986, in: B. Battrick, E. J. Rolfe & R. Reinhard (eds.), Exploration of Halley's Comet, ESA SP-250, ESTEC, Noordwijk vol. 2, p. 317
Schüller, F. 1930, IAU Circ. No. 288
Scotti, J. V. 1996, Minor Planet Circ. No. 26211
Sekanina, Z. 1976a, in: B. Donn, M. Mumma, W. Jackson, M. A'Hearn & R. Harrington (eds.), The Study of Comets, NASA SP-393, U. S. GPO, Washington, D. C., 1, 893
Sekanina, Z. 1976b, in: B. Donn, M. Mumma, W. Jackson, M. A'Hearn & R. Harrington (eds.), The Study of Comets, NASA SP- 393, U. S. GPO, Washington, D. C., p. 537
Sekanina, Z. 1977, Icarus 30, 574
Sekanina, Z. 1978, Icarus 33, 173
Sekanina, Z. 1979, Icarus 38, 300
Sekanina, Z. 1982, in: L. L. Wilkening (cd.), Comets, University of Arizona, Tucson, Ariz., p. 251
Sekanina, Z. 1988, AJ 95, 911, 970
Sekanina, Z. 1989a, AJ 98, 2322, 2377
Sekanina, Z. 1989b, IAU Circ. Nos. 4722, 4732
Sekanina, Z. 1991, AJ 102, 350
Sekanina, Z. 1995, IAU Circ. No. 6161
Sekanina, Z. 1996, IAU Circ. No. 6301
Stanton, R. H. 1981, J. Am. Assoc. Var. Star Obs. 10, 1
Sykes, M. V. & Walker, R. G. 1992, Icarus 95, 180
Tokunaga, A. T. & Hanner, M. S. 1985, ApJ 296, 1, 13
Weeder, G. J. & Hanner, M. S. 1987, AJ 94, 169
Wallis, M. K. 1986, in: O. Melita (cd.), Comet Nucleus Sample Return Mission, ESA SP - 249, ESTEC, Noordwijk, p. 63
Wirtz, C. (1930, Astron. Nachr. 240, 13